Applied Catalysis B: Environmental 180 (2016) 53–64

Contents lists available at ScienceDirect

Applied Catalysis B: Environmental

journal homepage: www.elsevier.com/locate/apcatb

Palladium nanoparticles supported on amine-functionalized SiO_2 for the catalytic hexavalent chromium reduction

Metin Celebi [a], Mehmet Yurderi [a], Ahmet Bulut [a], Murat Kaya [b], Mehmet Zahmakiran [a,*,1]

[a] Nanomaterials and Catalysis (NanoMatCat) Research Laboratory, Department of Chemistry, Yüzüncü Yıl University, 65080 Van, Turkey
[b] Department of Chemical Engineering and Applied Chemistry, Atilim University, 06836 Ankara, Turkey

ARTICLE INFO

Article history:
Received 28 April 2015
Received in revised form 3 June 2015
Accepted 11 June 2015
Available online 16 June 2015

Keywords:
Dichromate
Cr(VI)
Reduction
Pd
Nanocatalyst

ABSTRACT

Hexavalent chromium (Cr(VI)) is commonly identified acutely toxic, a proven mutagen and carcinogen heavy metal pollutant in the aquatic environment, whereas Cr(III) is believed to be an essential element. In the present study, we show that palladium(0) nanoparticles supported on 3-aminopropyltriethoxysilane (APTS) functionalized silica ($Pd@SiO_2–NH_2$) effectively catalyze the reduction of Cr(VI) to Cr(III) by using formic acid (HCOOH) as reducing agent under mild conditions (at room temperature under air). $Pd@SiO_2–NH_2$ catalyst was reproducibly prepared by deposition–reduction technique and characterized by the combination of various spectroscopic tools including ICP-OES, P-XRD, DR/UV–vis, XPS, BFTEM, HRTEM and TEM-EDX techniques. The sum of their results is indicative of the formation of well-dispersed palladium(0) nanoparticles (d_{mean} = 3.7 nm) on the surface of APTS-functionalized SiO_2. The catalytic performance of the resulting palladium(0) nanoparticles in terms of activity and stability was evaluated by the catalytic reduction of Cr(VI) to Cr(III) in aqueous solution in the presence of formic acid as a reducing agent. Our results reveal that $Pd@SiO_2–NH_2$ catalyst displays unprecedented activity (TOF = 258 mol $Cr_2O_7^{2-}$/mol Pd min) and reusability (<85% at 5th reuse) for the reduction of Cr(VI) to Cr(III) at room temperature. The present study reported here also includes the compilation of wealthy kinetic data for $Pd@SiO_2–NH_2$ catalyzed the reduction of Cr(VI) to Cr(III) in aqueous formic acid (HCOOH)–sodium formate (HCOONa) solution depending on substrate [$Cr_2O_7^{2-}$], catalyst [$Pd@SiO_2–NH_2$], surface grafted amine [APTS], formic acid [HCOOH], sodium formate [HCOONa] concentrations, temperature and type of support material (Al_2O_3, C, unmodified SiO_2) to understand the nature of the catalytic reaction and determine the rate expression and activation parameters.

1. Introduction

Hexavalent chromium (Cr(VI)) is well-known as an extremely serious and ubiquitous environmental pollutant produced in wastewaters by several industrial processes such as metal electroplating, leather tanning, pigment production, and wood preservation [1–4]. Cr(VI) is considered to be the third most common pollutant at hazardous waste sites and the second most abundant heavy metal contaminant [5]. In addition, Cr(VI) compounds have been proven to have acute toxicity, mutagenicity and carcinogenicity as well [6,7]. In their recent reports, the World Health Organization (WHO) has strictly regulated Cr(VI) level must be below 0.05 mg L^{-1} for drinking water [8]. In contrast, Cr(III) is much less toxic and less mobile in the nature and trace amounts of Cr(III) have been considered to be an essential nutrient for living organisms [9,10]. The reduction of Cr(VI) to Cr(III) is therefore the best opinion for Cr(VI) mitigation.

Up to date various catalytic materials have been tested in the reduction of Cr(VI) to Cr(III) to aid environmental remediation, including bacterium strains, Fe(II)-containing minerals, sulfides, ZnO nanorods and different organic structures [11–14]. Additionally, emerging as an important class of environmental catalytic materials, transition metal nanoparticles have received notable attention for their superior catalytic performances in recent years [15,16]. Of particular importance, the remarkable activities have also been achieved in the catalytic reduction of Cr(VI) over Pd based nanocatalysts such as PSA stabilized Pd nanoparticles (NPs) [17], PVP stabilized Pd nano-tetrapods [18] and amino-functionalized Pd nanowires [19] by using formic acid (FA; HCOOH) as a reducing agent. In these catalytic transformations FA undergoes a dehydrogenation to produce H_2 and CO_2 ($HCOOH \rightarrow CO_2 + H_2$) [20–23]. Then, H_2 adsorbed on the surface of these Pd NPs surface consequently reduces Cr(VI) to Cr(III) via a H_2 transfer pathway

* Corresponding author. Fax: +90 432 225 18 06.
E-mail address: zmehmet@yyu.edu.tr (M. Zahmakiran).
[1] Website: www.nanomatcat.com.

http://dx.doi.org/10.1016/j.apcatb.2015.06.020
0926-3373/

($Cr_2O_7^{2-} + 8H^+ + 3H_2 \rightarrow 2Cr^{3+} + 7H_2O$) [18,26]. However, these colloidal Pd NPs [17–19] tend to aggregate in their long time use because of the high surface energy. Meanwhile, isolation and reuse of these nanocatalysts is also very difficult. These drawbacks may greatly restrict the practical applications of these colloidal Pd nanocatalysts on environmental remediation. In this context, the incorporating of active Pd nanoparticles on or into solid matrices has already been acknowledged for preventing aggregation and facilitating recycling [5,24–28]. In these studies, different solid supports have been used for the immobilization of guest Pd NPs. For example, Yadav et al. [5] used MIL-101 metal-organic framework to stabilize Pd NPs for the removal of Cr(VI) from wastewater. Shen and co-workers [26] stabilized Pd NPs on electrospun polymer nanofibers and used them as recyclable catalytic material in the reduction of Cr(VI) to Cr(III) under mild conditions. Dandapat et al. [25] prepared γ-Al_2O_3 films by the hydrolysis followed by peptization of Al(OOH) and used them as host matrix for Pd NPs. The resulting supported Pd NPs show good stability throughout the reusability experiments in the Cr(VI) reduction using formic acid. However the preparation of the majority of these porous materials involves either complicated treatment or special instruments, which hinders their extensive application. Therefore, it is highly desirable to develop practical and applicable supported Pd NPs catalyst for the degradation of Cr(VI).

Aside from the selection of type of support material, the surface functionalization of support material is also another key factor for the improvement of the catalytic performance of surface supported Pd NPs in Cr(VI) reduction, in which FA is used as reducing agent [29]. For example, Xu and co-workers emphasized strong interaction between metal nanoparticles and amine group grafted on silica support in the catalytic FA dehydrogenation, which was named as "Strong Metal-Molecular Support Interaction" (SMMSI) [30]. After that, Mori et al. [31] reported that Pd NPs supported on $-N(CH_3)_2$ bearing resin provide better activity than that of supported on neat resin in FA dehydrogenation. They explained that the existence of surface bound $-N(CH_3)_2$ group facilitates the dissociation of O—H bond in FA and enhances dehydrogenation rate. In parallel to these findings, the results of our recent study [32] are showing that the physical mixture of Pd and MnO_x NPs supported on 3-aminpropyltriethoxysilane (APTS) functionalized silica acted as more active heterogeneous catalyst than that of supported on active carbon (C), nano-alumina (Al_2O_3), titania (TiO_2) and unmodified silica (SiO_2) in the FA dehydrogenation. The higher reactivity of Pd-MnO_x NPs supported on amine-grafted silica supports was assigned to the existence of $-NH_2$ group on the surface; ditto of Yamashita's work [31]. These results prompted us to use a previously unappreciated amine-grafted silica (SiO_2–NH_2) support material for guest surfactant-free Pd NPs in the catalytic reduction of Cr(VI) to Cr(III) using FA as we thought that the enhancement of Pd NPs activity in FA dehydrogenation also increases the rate of Cr(VI) reduction.

Palladium(0) nanoparticles supported on amine-grafted silica, hereafter reported as Pd@SiO_2–NH_2, were simply and reproducibly prepared through the conventional impregnation followed by simultaneous reduction method [33]. The characterization of Pd@SiO_2–NH_2 was done by using inductively coupled plasma-optical emission spectroscopy (ICP-OES), powder X-ray diffraction (PXRD), X-ray photoelectron spectroscopy (XPS), diffuse reflectance-UV–vis (DR/UV–vis), fourier transform infrared (FTIR), bright-field transmission electron microscopy (BFTEM), high resolution transmission electron microscopy (HRTEM), and transmission electron microscope-energy dispersive X-ray (TEM-EDX) techniques. Their results revealed that the formation of well-dispersed and highly crystalline 3.7 nm Pd NPs on the surface of amine-grafted silica. The resulting amine-grafted silica supported Pd NPs provide unprecedented activity (TOF = 258 mol $Cr_2O_7^{2-}$/mol Pd min) in the catalytic reduction of Cr(VI) to Cr(III) using FA at room temperature. In addition to their high activity, they also show high stability against leaching and sintering throughout the catalytic runs, which make them highly reusable catalyst (retains >85% at 5th reuse) for this catalytic transformation.

2. Experimental

2.1. Materials

Palladium(II) nitrate dihydrate ($Pd(NO_3)_2{\cdot}2H_2O$) (~40% Pd basis), silica gel (40–63 μm), 3-aminopropyltriethoxysilane ($H_2N(CH_2)_3Si(OC_2H_5)_3$), sodium borohydride ($NaBH_4$), ninhydrin ($C_9H_6O_4$), ethanol ($C_2H_5OH$), potassium dichromate ($K_2Cr_2O_7$) and sodium hydroxide (NaOH) were purchased from Sigma–Aldrich®. Deionized water was distilled by water purification system (Milli-Q Water Purification System). All glassware and Teflon-coated magnetic stir bars were washed with acetone and copiously rinsed with distilled water before drying in an oven at 323 K.

2.2. Characterization

Palladium content of the samples was determined by ICP-OES (Leeman, Direct Reading Echelle) after each sample was completely dissolved in a mixture of HNO_3/HCl (1/3 ratio). Powder X-ray diffraction (XRD) patterns were recorded with a MAC Science MXP 3TZ diffractometer using Cu-Kα radiation (wavelength 1.54 Å, 40 kV, 55 mA). BFTEM and HRTEM samples were prepared by dropping one drop of dilute suspension on copper coated carbon TEM grid and the solvent was then dried. The BFTEM was carried out on a JEOL JEM-200CX transmission electron microscopes operating at 120 kV. Oxford EDXS system and Inca software were used to collect and process -TEM-EDX data. HRTEM was run on a JEOL JEM-2010F transmission electron microscope operating at 200 kV. The XPS analyses were performed on a Physical Electronics 5800 spectrometer equipped with a hemispherical analyzer and using monochromatic Al- Kα radiation (1486.6 eV, the X-ray tube working at 15 kV and 350 W, and pass energy of 23.5 eV). The gas generated from the decomposition of formic acid was analyzed by Shimadzu FID-2014 and TCD-2014 GC analyzers. The FTIR spectra of the gas generated from the decomposition of formic acid and SiO_2–NH_2 samples were taken on Shimadzu IR-Affinity-1. DR/UV–vis and UV–vis spectra were taken by using Shimadzu UV-2600 with integrating sphere attachment. nitrogen adsorption/desorption experiments were carried out at 77 K using a NOVA 3000 series (Quantachrome Instruments) Instrument.

2.3. Preparation of SiO_2–NH_2

Prior to the functionalization procedure, the silica sample was dried in vacuum oven at 393 K under 10^{-1} Torr pressure overnight to remove any physisorbed water. Afterwards, the functionalization of SiO_2 was carried out by adding a desired amount of APTS to 30 mL of dry ethanol containing SiO_2. The resulting slurry was allowed to stir for 12 h. The white solid was filtered by using Whatmann filter paper and washed repeatedly with dry ethanol. The white amine-functionalized silica (SiO_2–NH_2) powders was dried in a vacuum oven at 373 K under 10^{-1} Torr pressure and used for further application. The presence of $-NH_2$ groups on SiO_2 support was quantified by the colorimetric ninhydrin method as described elsewhere [34].

2.4. Preparation of Pd@SiO_2–NH_2

Pd@SiO_2–NH_2 catalyst was obtained by the conventional impregnation and subsequent reduction steps [33]. Typically, 5.0 mL aqueous solution containing $Pd(NO_3)_2{\cdot}2H_2O$ (7.40 mg,

28.7 μmol Pd) and SiO_2–NH_2 (100 mg, 100 μmol NH_2) is mixed for 3 h. Then, the fresh 1.0 mL aqueous solution of $NaBH_4$ (16 mg, 0.43 mmol) was added to this mixture and the resulting solution was stirred for half an hour under ambient conditions. After centrifugation (6000 rpm, 5 min), copious washing with water (3 × 20 mL), filtration, and drying in oven at 373 K, Pd@SiO_2–NH_2 catalyst was obtained as a dark gray powder.

2.5. Preparation of Pd@C, Pd@Al_2O_3 and Pd@SiO_2 catalysts

In a three separate experiments 5.0 mL aqueous solution containing $Pd(NO_3)_2 \cdot 2H_2O$ (7.40 mg, 28.7 μmol Pd) and solid support (100 mg C, Al_2O_3, SiO_2) is mixed for 3 h. After that, the fresh aqueous $NaBH_4$ solution (1.0 mL, 16 mg, 0.43 mmol) was added to these mixtures and the resulting solutions were stirred for half an hour under ambient conditions. After centrifugation (6000 rpm, 5 min), copious washing with water (3 × 20 mL), filtration, and drying in oven at 373 K, Pd@C, Pd@Al_2O_3 and Pd@SiO_2 catalysts were obtained as powders.

2.6. Identification of gaseous products from the decomposition of formic acid in the presence of Pd@SiO_2–NH_2 catalyst

Before starting the catalytic decomposition of FA, a jacketed one necked reaction flask (50.0 mL) containing a Teflon-coated stir bar was placed on a magnetic stirrer (Heidolph MR-3004) and thermostated to 298 K by using a constant temperature bath (Lab Companion RW-0525). In a typical experiment, Pd@SiO_2–NH_2 catalyst was weighed and transferred into the reaction flask, and then 9.0 mL H_2O was added into the reaction flask and this mixture was stirred for 15 min to achieve thermal equilibrium. Next, 1.0 mL aqueous FA solution (0.45 M FA + 0.45 M SF) was added into the reaction flask via its septum by using a 1.0 mL gastight syringe and the catalytic reaction was started (t = 0 min) by stirring the mixture at >600 rpm. The gas generated from the decomposition of FA was collected by GC balloon and FTIR gas sample holder to analyze by Shimadzu TCD-2014GC analyzer and Shimadzu IR-Affinity-1, respectively.

2.7. Sodium hydroxide (NaOH) trap experiment

In order to determine CO_2/H_2 molar ratio in the gas mixture generated during the Pd@SiO_2–NH_2 catalyzed decomposition of 10.0 mL aqueous FA solution (0.45 M FA + 0.45 M SF), NaOH trap experiment was performed as described elsewhere [21,23]. In this experiment, the trap (10.0 M NaOH solution) was placed between the jacketed reactor and gas burette. The generated gas during the reaction was passed through the NaOH trap to capture generated CO_2. Then, the volume of the gas generated from the decomposition of FA was monitored and compared to those without trap experiment. We observed that the volume of the generated gas decreased by a factor of two in the presence of the NaOH, trap. This result is indicative of the complete adsorption of CO_2 in NaOH solution ($2NaOH + CO_2 \rightarrow Na_2CO_3 + H_2O$) and the presence of equivalent molar amounts of CO_2 and H_2 (1.0:1.0) in the product mixture of the Pd@SiO_2–NH_2 FA decomposition.

2.8. Catalytic performance of Pd@SiO_2–NH_2 in the catalytic reduction of Cr(VI) to Cr(III)

2.8.1. Catalysis experiments

A mixture containing water (10.0 mL), $K_2Cr_2O_7$ (2.0 mM, 5.89 mg), HCOOH (0.45 M, 173.2 μL), HCOONa (0.45 M, 312.3 mg) was taken in a jacketed one necked reaction flask (50.0 mL) containing a Teflon-coated stir bar was placed on a magnetic stirrer (Heidolph MR-3004) and thermostated to 298 K by using a constant temperature bath (Lab Companion RW-0525). Then, the mixture was stirred for 15 min to achieve thermal equilibrium. Next, the catalyst was weighed and transferred into the reaction flask and the catalytic reaction was started (t = 0 min) by stirring the mixture at >600 rpm. At each predetermined time interval 100 μL of the reaction solution was withdrawn and diluted to 1.0 mL for the analysis of transformation efficiency of Cr(VI) to Cr(III) using a Shimadzu UV-2600 UV–vis spectrometer.

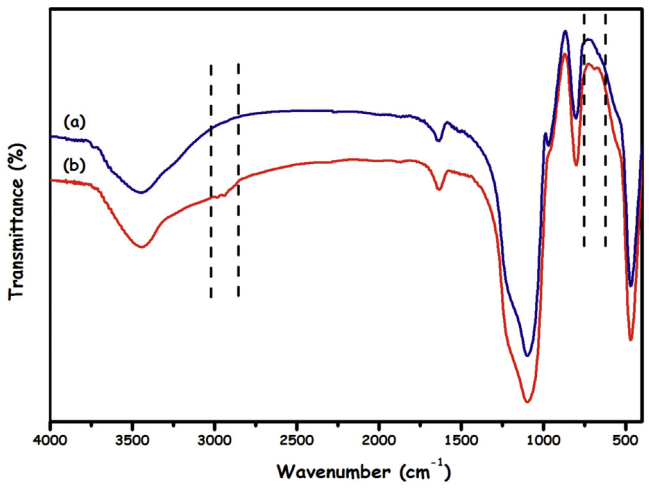

Fig. 1. FTIR spectrum of (a) SiO_2 (unmodified), (b) APTS grafted SiO_2 (SiO_2–NH_2) in the range of 4000–400 cm^{-1}.

2.8.2. UV–vis spectroscopic studies of the reduction products

The optical absorption spectra were measured at a fixed wavelength 350 nm, which is the characteristic absorption peak for Cr(VI). The concentration of Cr(VI) was calculated using a calibration curve constructed with absorbance of standard solutions. The extent of catalytic reduction was expressed as conversion, which was calculated as Eq. (1) shows:

$$\text{Conversion} = \frac{[\text{Cr(VI)}]}{[\text{Cr(V1)}]_0} \quad (1)$$

where $[Cr(IV)]_0$ is the initial concentration and [Cr(VI)] is the concentration at certain time point.

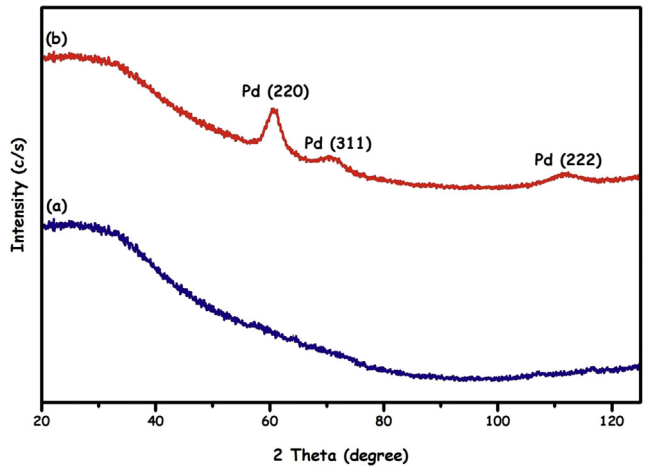

Fig. 2. P-XRD patterns of (a) SiO_2–NH_2, (b) Pd@SiO_2–NH_2 in the range of 2θ = 20–122°.

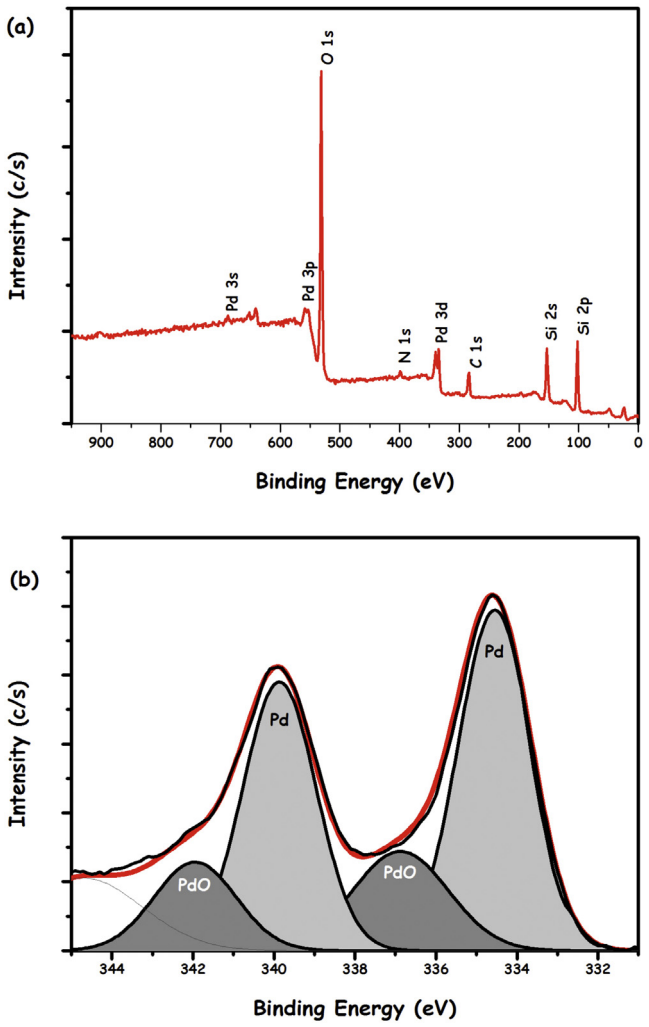

Fig. 3. (a) Survey XPS spectrum, (b) High resolution Pd 3d XPS spectrum of Pd@SiO_2–NH_2.

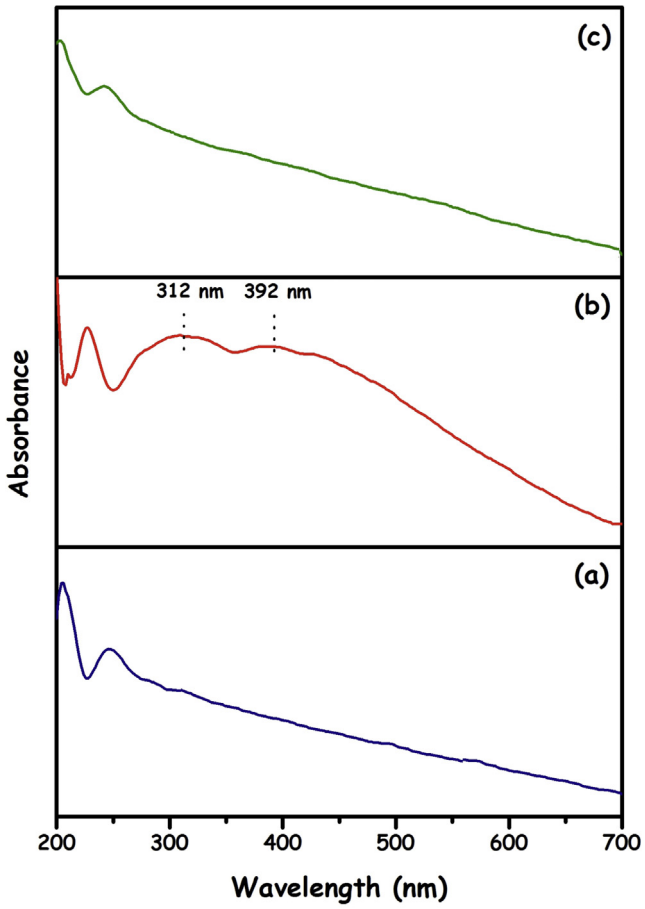

Fig. 4. DR/UV–vis spectra of (a) SiO_2–NH_2, (b) Pd^{2+}@SiO_2–NH_2, (c) Pd@SiO_2–NH_2 in the range of 200–700 nm.

2.8.3. Confirmation of Cr(III) as a reaction product

The presence of Cr(III) as the sole reaction product was confirmed using sodium hydroxide. An excess of sodium hydroxide was added at the end of the reaction to a solution of hexaaquachromium(III) ions, a green solution of hexahydroxochromate(III) was produced, which confirms that the presence of Cr(III) [35].

2.8.4. Effect of surface grafted amine loadings

In a set of experiments the catalytic reduction of Cr(VI) to Cr(III) in an aqueous solution containing water (10.0 mL), $K_2Cr_2O_7$ (2.0 mM, 5.89 mg), HCOOH (0.45 M, 173.2 μL), HCOONa (0.45 M, 312.3 mg) at 298 K was performed by using Pd NPs supported on SiO_2 that functionalized with various amounts of amine group (0.0, 1.0, 2.4 and 4.6 mmol NH_2/g SiO_2).

2.8.5. Reusability performance

After one complete reaction cycle, the catalyst was isolated by suction filtration using Whatmann filter paper and washed with excess ethanol–water mixture and dried in vacuum–oven at 373 K (10^{-1} Torr). Then, the dried catalyst weighed and used for the next cycle of catalytic reaction with fresh substrates.

2.9. Kinetic studies for the catalytic reduction of Cr(VI) to Cr(III) over Pd@SiO_2–NH_2 catalyst

The kinetic studies for the catalytic reduction of Cr(VI) to Cr(III) over Pd@SiO_2–NH2 catalyst were performed depending on different parameters including [$Cr_2O_7^{2-}$], [Pd], [HCOOH], [HCOONa] and temperature (see below) by following the same experimental procedure given in the Section of 2.8.1.

2.9.1. Effect of dichromate concentration [$Cr_2O_7^{2-}$]

Pd@SiO_2–NH_2 (10 mg; 1.4 wt% Pd corresponds to 1.32 μmol Pd) catalyzed reduction of Cr(VI) to Cr(III) was performed in an aqueous solution containing water (10.0 mL), HCOOH (0.45 M, 173.2 μL), HCOONa (0.45 M, 312.3 mg) at 298 K starting with various $K_2Cr_2O_7$ concentrations (1.0, 2.0, 4.0 and 6.0 mM).

2.9.2. Effect of catalyst concentration [Pd NPs]

In another set of experiments the catalytic reduction of Cr(VI) to Cr(III) in an aqueous solution containing water (10.0 mL), $K_2Cr_2O_7$ (2.0 mM, 5.89 mg), HCOOH (0.45 M, 173.2 μL), HCOONa (0.45 M, 312.3 mg) was performed at different Pd NPs concentrations (5.0, 7.5, 10.0 and 15.0 mg Pd@SiO_2–NH_2 with 1.4 wt% Pd loadings corresponds to 0.066, 0.099, 0.132, 0.198 mM Pd) and 298 K.

2.9.3. Effect of formic acid concentration [HCOOH]

The effect of FA concentration as reducing agent was investigated through a set of experiments in which the Pd@SiO_2–NH_2 (10 mg; 1.4 wt% Pd corresponds to 1.32 μmol Pd) catalyzed reduc-

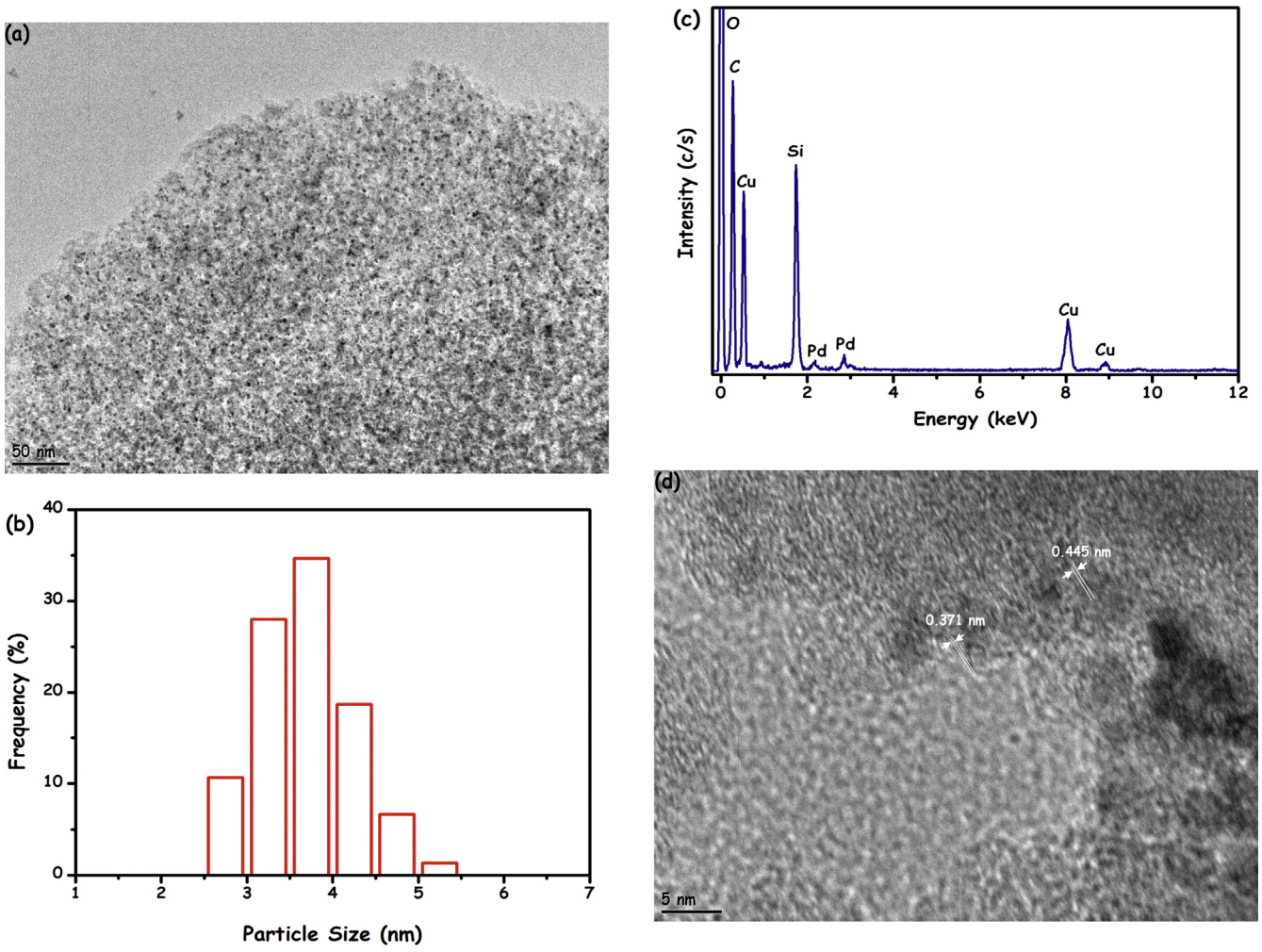

Fig. 5. (a) BFTEM image of Pd@SiO_2–NH_2 and corresponding size histogram of resulting Pd NPs (b), (c) TEM-EDX spectrum of Pd@SiO_2–NH_2 catalyst, (d) HRTEM image of Pd@SiO_2–NH_2 catalyst.

tion of Cr(VI) in an aqueous solution (10.0 mL; $K_2Cr_2O_7$ 2.0 mM, 5.89 mg; HCOONa 0.45 M, 312.3 mg) was performed at 298 K and different FA concentrations (0, 122.5 mM, 225, 450 and 675 mM).

2.9.4. Effect of sodium formate concentration [HCOOH]

The effect of SF concentration as a promoter was also investigated by performing a series of experiments for Pd@SiO_2–NH_2 (10 mg; 1.4 wt% Pd corresponds to 1.32 μmol Pd) catalyzed reduction of Cr(VI) in an aqueous solution (10.0 mL; $K_2Cr_2O_7$ 2.0 mM, 5.89 mg; HCOOH 0.45 M, 173.2 μL) at 298 K and various SF concentrations (0, 122.5, 225, 450 and 675 mM).

2.9.5. Effect of temperature

In order to determine the activation parameters (Ea, ΔH^* and ΔS^*) for the Pd@SiO_2–NH_2 (10 mg; 1.4 wt% Pd corresponds to 1.32 μmol Pd) catalyzed reduction of Cr(VI) in an aqueous solution containing water (10.0 mL), $K_2Cr_2O_7$ (2.0 mM, 5.89 mg), HCOOH (0.45 M, 173.2 μL), HCOONa (0.45 M, 312.3 mg). The catalytic reaction was performed at different temperatures in the range of 298–318 K and the initial rate constants were determined and used to construct Arrhenius and Eyring–Polonyi plots to find activation parameters.

2.10. The uniqueness of Pd@SiO_2–NH_2 catalyst in the catalytic reduction of Cr(VI) to Cr(III)

To investigate the uniqueness of Pd@SiO_2–NH_2 with respect to Pd@C, Pd@Al_2O_3 and Pd@SiO_2 catalysts; the catalytic reduction of Cr(VI) to Cr(III) was performed in a set of experiments under identical conditions (10.0 mL; $K_2Cr_2O_7$ 2.0 mM, 5.89 mg; HCOONa 0.45 M, 312.3 mg, [Pd] = 0.132 mM) by using Pd@C, Pd@Al_2O_3 and Pd@SiO_2 catalysts at 298 K.

3. Results and discussion

3.1. The preparation and characterization of Pd NPs supported on the amine-functionalized silica

Before the preparation of Pd@SiO_2–NH_2, APTS functionalization of SiO_2 support material was done by refluxing of APTS and activated SiO_2 in dry ethanol. The grafting of APTS onto SiO_2 support was evidenced by FTIR spectroscopy and quantified by ninhydrin method (*vice versa*) [34]. Fig. 1 shows FTIR spectra of SiO_2 (unmodified) and APTS grafted-SiO_2. The comparison of two spectra reveals that the post-grafting of APTS onto SiO_2, which is confirmed by the appearance of several new peaks in the ranges of 3000–2800 cm^{-1} and 750–650 cm^{-1} due to C—H stretching and N—H bending vibrations of APTS, respectively [36]. Afterwards, palladium NPs supported on 3-

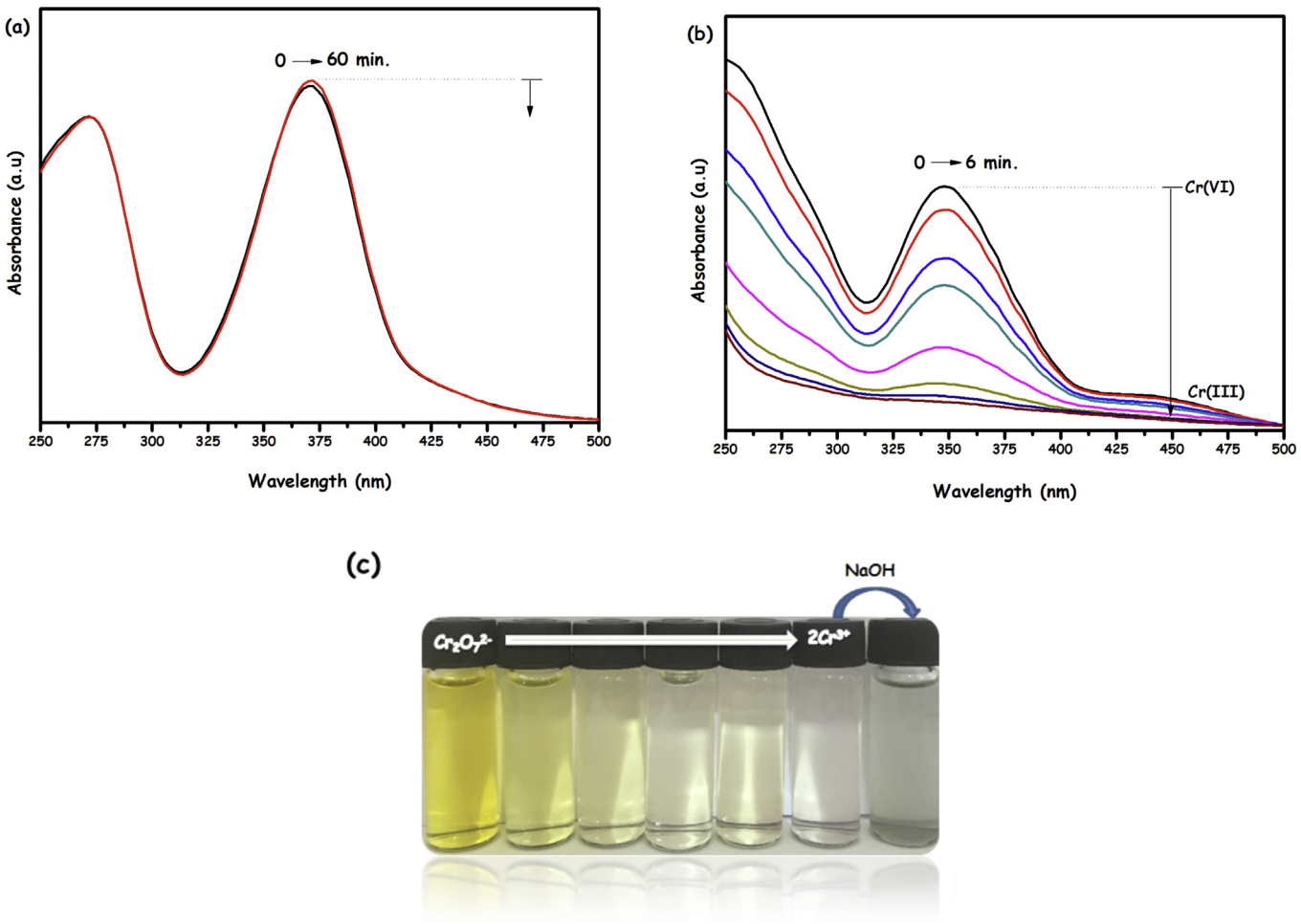

Fig. 6. UV–vis spectra for the reduction of Cr(VI) to Cr(III) by using FA ($K_2Cr_2O_7$ 2.0 mM, HCOOH 0.45 M, HCOONa 0.45 M in 10.0 mL H_2O) in the presence of (a) SiO_2–NH_2 (10 mg), (b) Pd@SiO_2–NH_2 (10 mg with 1.40 wt% Pd; 1.32 μmol Pd) at 298 K, (c) the photographs of reaction solution for Pd@SiO_2–NH_2 catalyzed reduction of Cr(VI) to Cr(III) by using FA and formation of green hexahydroxochromate solution by addition of excess NaOH.

aminopropyltriethoxysilane functionalized silica (Pd@SiO_2–NH_2) were simply and reproducibly prepared by following the procedure comprising of the conventional impregnation of Pd(II) onto support and its subsequent $NaBH_4$ reduction in water all at room temperature. After centrifugation, copious washing with water, and drying under vacuum Pd@SiO_2–NH_2 catalyst was obtained as powders and characterized by ICP-OES, P-XRD, XPS, DR/UV–vis, BFTEM, HRTEM, TEM-EDX and N_2-adsorption–desorption techniques.

The palladium and free amine content of the as-prepared catalyst was found to be 1.40 wt% Pd and 0.98 mmol NH_2/g SiO_2 by ICP-OES analyses and ninhydrin method [23], respectively. The specific BET surface areas for SiO_2 and Pd@SiO_2–NH_2 were found to be 360 and 312 m^2/g, respectively. The decrease in the surface area can be attributed to existence of Pd NPs on the surface of APTS-functionalized SiO_2. P-XRD patterns of Pd@SiO_2–NH_2 and SiO_2–NH_2 are given in Fig. 2. Pd@SiO_2–NH_2 shows the diffraction lines of Pd (220), (311) and (222) planes at 61, 71 and 112°, respectively (JCPDS No. 05-0681) [37]. In order to determine the chemical environment and oxidation state of palladium on Pd@SiO_2–NH_2 we performed survey and Pd 3d core level XPS measurements (Fig. 3). Fig. 3(a) shows the survey XPS survey spectrum of Pd@SiO_2–NH_2 that reveals the existence of SiO_2–NH_2 elements (Si, N, C, O) and Pd in the sample. The deconvulation of Pd 3d XPS spectrum gives distinctive peaks at 334.5 and 339.8 eV, which can readily be assigned to Pd^0 $3d_{5/2}$ and Pd^0 $3d_{3/2}$, respectively for metallic palladium (Pd(0)) [38]. The peaks observed at 336.9 and 341.9 eV can be attributed to Pd^{2+} $3d_{5/2}$ and Pd^{2+} $3d_{3/2}$, respectively and reveals the presence of PdO, which may originate from the surface oxidation of palladium(0) nanoparticles during the XPS sampling procedure [39]. In addition to XPS, we also performed DR/UV–vis analyses on SiO_2–NH_2, Pd^{2+}@SiO_2–NH_2 and Pd@SiO_2–NH_2 to check whether PdO is really formed during the XPS sampling procedure or in the preparation of Pd@SiO_2–NH_2. Fig. 4 shows DR/UV–vis spectra of SiO_2–NH_2, Pd^{2+}@SiO_2–NH_2 and Pd@SiO_2–NH_2 samples. DR/UV–vis spectrum of Pd^{2+}@SiO_2–NH_2 shows absorption peaks at about 312 and 392 nm, characteristics of Pd^{2+} [40], whereas SiO_2–NH_2 and Pd@SiO_2–NH_2 spectra were found to be identical. The absence of the absorption peaks above 300 nm in Pd@SiO_2–NH_2 sample indicative of the full reduction of Pd^{2+}@SiO_2–NH_2 to Pd@SiO_2–NH_2, which confirms that the detection of PdO by XPS is resulting from the surface oxidation of palladium(0) nanoparticles during the XPS sampling procedure.

The size, morphology and surface composition of Pd@SiO_2–NH_2 were investigated by BFTEM, HRTEM and TEM-EDX analyses. BFTEM image of Pd@SiO_2–NH_2 catalyst (1.40 wt% Pd) is given in Fig. 5(a), which shows the presence of well-dispersed Pd NPs in the range of 2.5–5.2 nm with a mean diameter of 3.7 nm (Fig. 5(b)). EDX analysis performed during the TEM observation of Pd@SiO_2–NH_2 catalyst from many different areas confirmed the presence of Pd metal in the analyzed regions (Fig. 5(c)). HRTEM image of Pd@SiO_2–NH_2 catalyst given in Fig. 5(d) discloses the highly crystalline nature of resulting Pd NPs, the lattice spacing distances of two individual spherical Pd NPs were measured to be 0.371 and

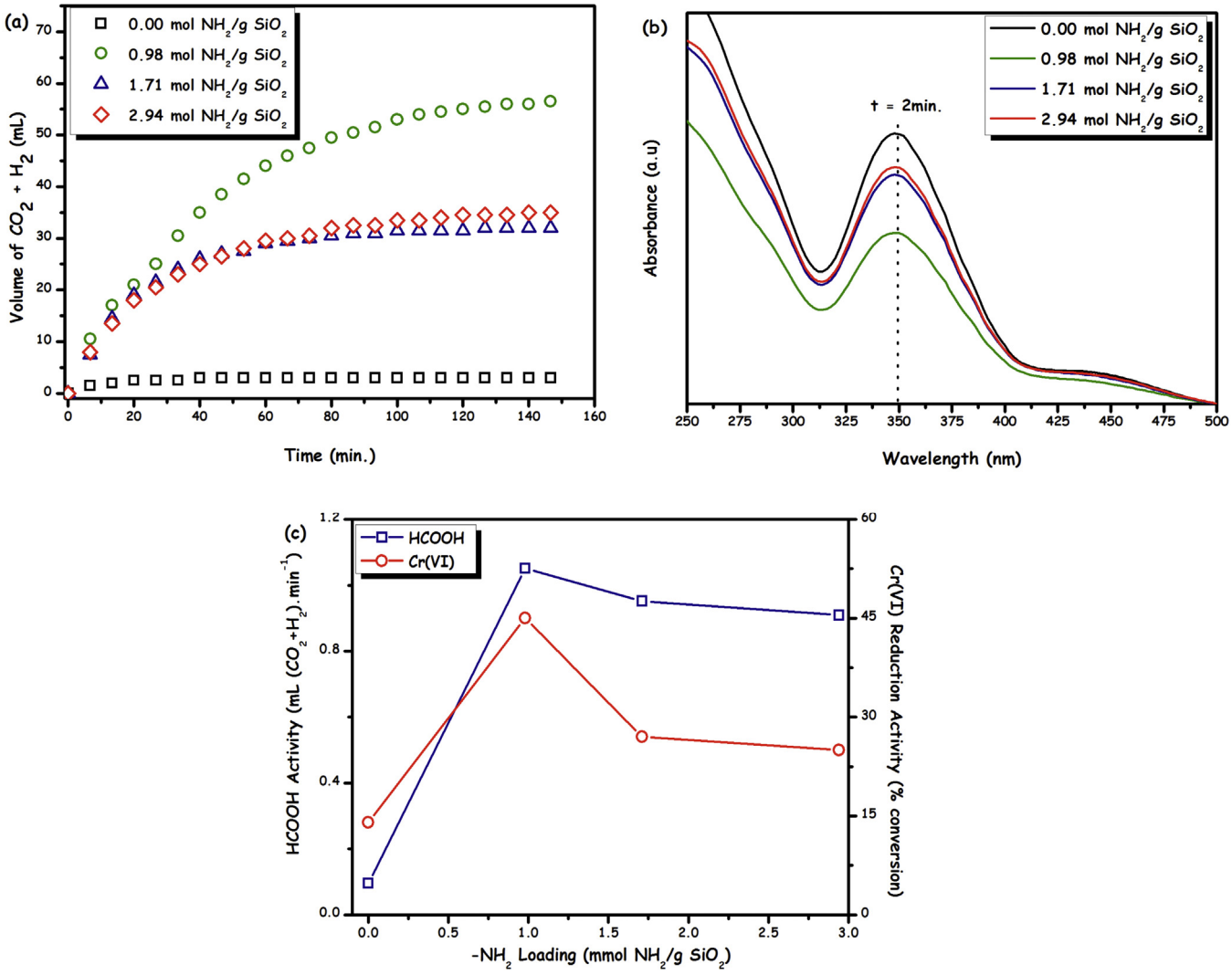

Fig. 7. (a) The volume of the generated gas ($CO_2 + H_2$) *versus* time graph for the room temperature dehydrogenation of FA (HCOOH 0.25 M, HCOONa 0.25 M in 10.0 mL H_2O) over Pd@SiO_2–NH_2 catalysts (100 mg Pd@SiO_2–NH_2 with 1.40 wt% Pd loading were used corresponds to 13.2 μmol Pd in all catalysts), which were functionalized with different amounts of amine groups at same Pd concentration, (b) UV–vis spectra for the catalytic reduction of Cr(VI) to Cr(III) ($K_2Cr_2O_7$ 2.0 mM, HCOOH 0.45 M, HCOONa 0.45 M in 10.0 mL H_2O) over the same Pd@SiO_2–NH_2 catalyst (10.0 mg with 1.40 wt% Pd; 1.32 μmol Pd in all catalysts) given in (a) at 298 K, (c) the observed catalytic activities in the dehydrogenation of FA and Cr(VI) reduction depending on the amount of amine groups exist on the SiO_2 support.

0.445 nm, which corresponds to Pd (2 2 0) and Pd (2 2 2) crystalline fringes, respectively [41–44].

3.2. The control experiments for the decomposition of formic acid over Pd@SiO_2–NH_2 catalyst

In our designed system for the catalytic reduction of Cr(VI) to Cr(III) over Pd@SiO_2–NH_2 catalyst, we used sodium formate (SF) as a promoter to enhance the rate of formic acid decomposition as reported in many reports [20–23]. In this context, the recent reports have pointed out that some homogeneous [43] and heterogeneous [28] catalysts can liberate H_2 not only from FA but also SF through a catalytic hydrolysis of SF ($HCOONa + H_2O \rightarrow H_2 + NaHCO_3$). For this reason we first performed a control experiment to check whether Pd@SiO_2–NH_2 catalyze the hydrolysis of SF. The result of this experiment showed that Pd@SiO_2–NH_2 catalyzed hydrolysis of SF only produces 2.5 mL hydrogen gas over 3.5 h even at 318 K.

A series of control experiments were also done for the identification of the generated gas from Pd@SiO_2–NH_2 catalyzed decomposition of FA, since dehydrogenation of FA ($HCOOH \rightarrow CO_2 + H_2$) is generally associated with the dehydration ($HCOOH \rightarrow H_2O + CO$) [45]. At this concern, it is important to know that the exact reducing agent in the Cr(VI) reduction as both H_2 [46] and CO [47] can act as a reducing agent for the reduction of metal complexes. For that purpose the generated gas over Pd@SiO_2–NH_2 catalyst was identified by GC, FTIR and NaOH trap experiment [20–23]. The results of these control experiments (Figs. S1–S3) revealed that the generated gas is a mixture of H_2 and CO_2 with a H_2:CO_2 molar ratio of 1.0:1.0 where CO was below the detection limit (*i.e.* <10 ppm).

3.3. Catalytic performance of Pd@SiO_2–NH_2 in the reduction of Cr(VI) to Cr(III)

3.3.1. The monitoring the catalytic reaction and the catalytic reactivity of palladium-free APTS-functionalized SiO_2

The catalytic performance of Pd@SiO_2–NH_2 catalyst was investigated in the catalytic reduction of Cr(VI) to Cr(III) by using FA as reducing agent. Potassium dichromate ($K_2Cr_2O_7$) was chosen as one the representative Cr(VI) compounds. It is well-known that the characteristics absorption peak of Cr(VI) is centered at 350 nm, which originates from the ligand (oxygen) to metal (Cr(VI)) charge

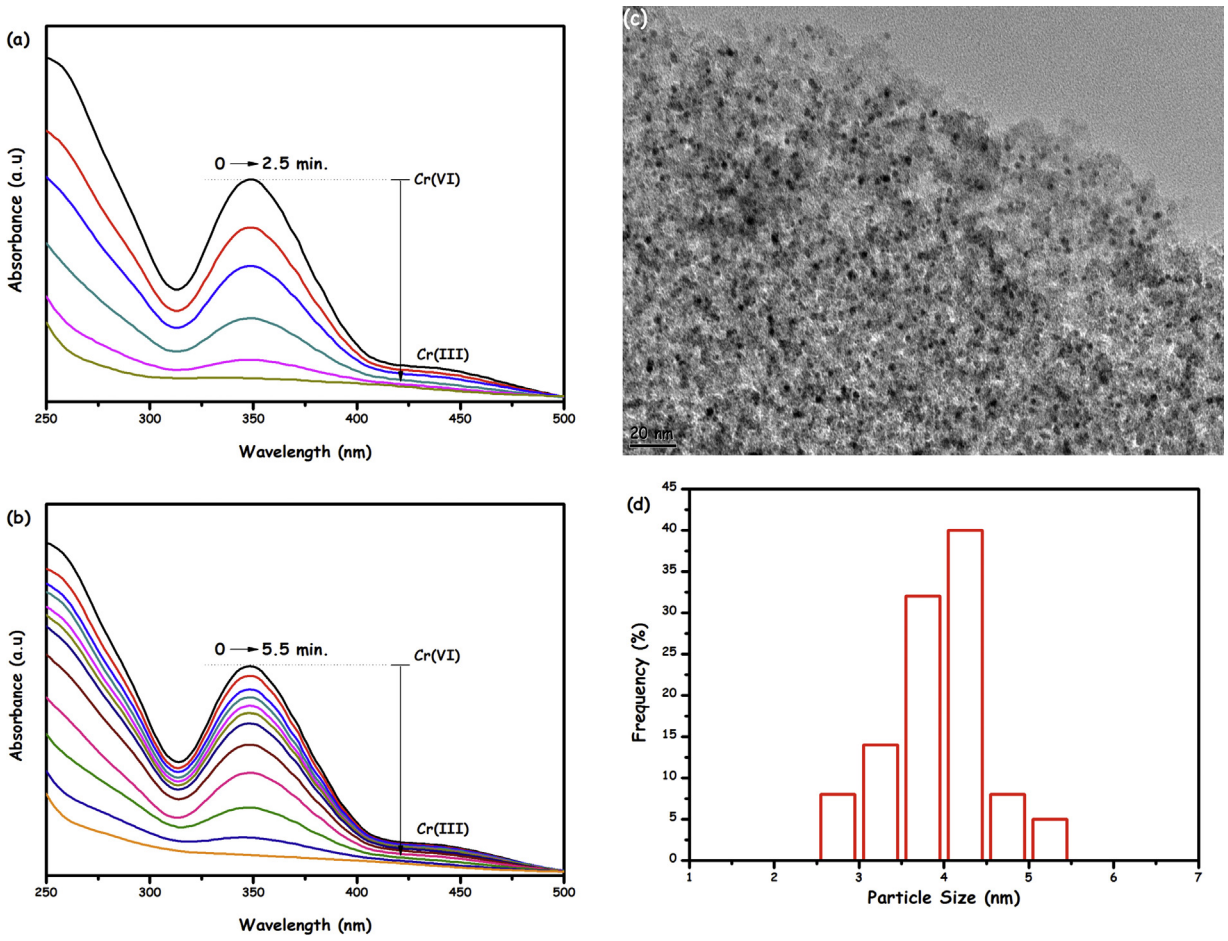

Fig. 8. UV–vis spectra for the catalytic reduction of Cr(VI) to Cr(III) ($K_2Cr_2O_7$ 2.0 mM, HCOOH 0.45 M, HCOONa 0.45 M in 10.0 mL H_2O) over (a) 15.0 mg Pd@SiO_2–NH_2 catalyst (1.40 wt% Pd; 1.98 μmol Pd) in the 1st run, (b) 8.0 mg Pd@SiO_2–NH_2 catalyst (1.40 wt% Pd; 1.06 μmol Pd) in the 5th run, (c) BFTEM image of Pd@SiO_2–NH_2 catalyst recovered after 5th catalytic reuse and (d) its corresponding size histogram.

transfer transition (LMCT) [24–28]. Thus the reduction processes can be monitored by UV–vis spectroscopy. Before testing the catalytic activity of Pd@SiO_2–NH_2 catalyst in the catalytic reduction of Cr(VI) to Cr(III), the catalytic reactivity of APTS-functionalized SiO_2 (SiO_2–NH_2) as host material was checked under identical conditions (*vide infra*). In the absence of Pd metal, the absorption intensity at 350 nm remains almost unchanged over 60 min (Fig. 6(a)), suggesting that the catalytic reduction cannot be proceed without Pd. When an ultralow amount of Pd NPs on SiO_2–NH_2 (10.0 mg Pd@SiO_2–NH_2 with 1.40 wt% Pd loading corresponds to 1.32 μmol Pd) support was introduced, the absorption peak at 350 nm gradually decreased and vanished within 6 min (Fig. 6(b)), accompanying a color change of yellow to colorless (Fig. 6(c)) indicating the reduction of Cr(VI) at room temperature. The formation of Cr(III) was also confirmed by adding an excess of NaOH, where the color of solution changed from colorless to green indicating the formation of hexahydroxochromate(III). The pH of solution throughout the Pd@SiO_2–NH_2 catalyzed reduction of Cr(VI) to Cr(III) in the presence of FA was also monitored and found that pH value increased from 3.64 to 3.68 at an initial stage of the reaction and remained constant at this pH value to the end of the reaction (Fig. S4).

3.3.2. Effect of APTS loading on the catalytic activity of Pd@SiO_2–NH_2 and uniqueness of Pd@SiO_2–NH_2 in the catalytic reduction of Cr(VI) to Cr(III)

As we discussed in the introduction section, the recent studies for the catalytic dehydrogenation of FA have showed that the existence amine groups of surface bound APTS enhances the rate of FA dehydrogenation by facilitating the dissociation of O—H bond in FA [30,31]. In this context we compared the catalytic activities Pd@SiO_2–NH_2, which were functionalized with different amounts of amine groups, in both FA dehydrogenation and Cr(VI) reduction to understand the effect of the surface-grafted amine functionalities on the catalytic reactivity of Pd NPs in both of these catalytic reactions. Fig. 7(a) shows the volume of generated gas ($CO_2 + H_2$) *versus* the reaction time and for FA dehydrogenation in the presence of Pd@SiO_2–NH_2 catalysts, which were functionalized with different amounts of amine groups, at 298 K. We found that amine-free SiO_2 supported Pd NPs provides the lowest gas generation rate (0.095 mL/min) and the catalytically optimum amine loading is 0.98 mmol NH_2/g SiO_2, where the maximum gas generation rate can be achieved by Pd@SiO_2–NH_2 (1.051 mL/min). Then, the same catalytic materials were used in the catalytic reduction of Cr(VI) to Cr(III) by using FA at 298 K. Fig. 7(b) shows UV–vis spectra of the reaction solutions taken at t = 2 min. of these catalytic transformations. Expectedly, we observed that amine-free SiO_2 supported Pd NPs provides the lowest conversion (14%) within the considered time interval and the catalytically best amine loading was again found to be 0.98 mmol NH_2/g SiO_2, in which the maximum conversion (45%) at 2 min. can be achieved.

As seen from Fig. 7(c) the amount of amine loading leads to the observation of the same trend in the catalytic activities of Pd@SiO_2–NH_2 catalysts for both of the dehydrogenation of FA and the reduction of Cr(VI) to Cr(III) by using FA. The limited reactivity of Pd NPs supported on amine-free SiO_2 can be explained by the

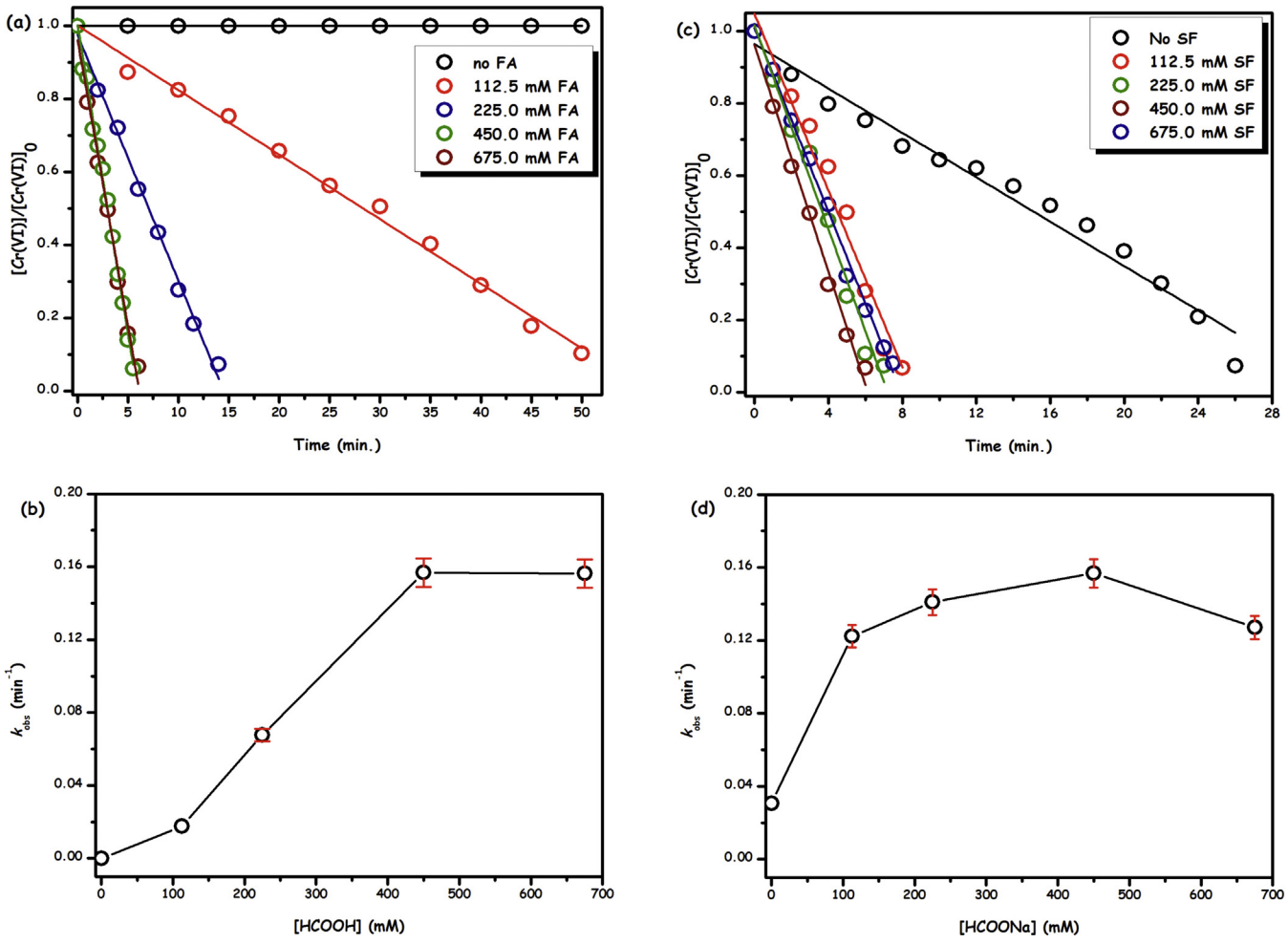

Fig. 9. (a) The remaining fraction of Cr(VI) ($[Cr(VI]/[Cr(VI)]_0$) *versus* time graph and corresponding (b) observed rate constants *versus* FA concentration depending on [HCOOH], (c) the remaining fraction of Cr(VI) ($[Cr(VI]/[Cr(VI)]_0$) *versus* time graph and corresponding (d) observed rate constants *versus* SF concentration depending on [HCOONa] for the catalytic reduction of Cr(VI) to Cr(III) ($K_2Cr_2O_7$ 2.0 mM in 10.0 mL H_2O) over Pd@SiO_2–NH_2 catalyst (10 mg with 1.40 wt% Pd; 1.32 μmol Pd) at 298 K.

absence of $-NH_2$ functionalities on the support material, which may have a direct impact not only on the FA adsorption/storage process as explained above but also the nucleation and growth of the Pd NPs [48,49] on the support surface as the BFTEM image of Pd NPs supported on amine-free SiO_2 (Fig. S5) clearly shows that the formation of Pd agglomerates on the support surface. On the other hand, the lower activities observed at high amine loadings (*i.e.* >1 mmol NH_2/g SiO_2), which provide smaller Pd NPs (3.2 nm; Fig. S6), can be attributed the poisoning of the Pd NPs by the excessive amount of surface $-NH_2$ functionalities that cover active surfaces of Pd NPs [48,49]. For all other test reactions conducted in this study samples of Pd@SiO_2–NH_2 containing ~0.98 mmol NH_2/g SiO_2 were used. The influence of the type of the support material was also investigated by synthetically replacing SiO_2–NH_2 with some of the ubiquitous support materials used in catalysis such as Al_2O_3 and C. The catalytic activities of Pd@SiO_2–NH_2 (1.40 wt% Pd), Pd@Al_2O_3 (1.42 wt% Pd) and Pd@C (1.39 wt% Pd) catalysts prepared by the same method were investigated in the catalytic reduction of Cr(VI) to Cr(III) under identical conditions (Figs. S7 and S8). The percent conversions (%) at t = 2.0 min. were observed to decrease in the following order: Pd@SiO_2–NH_2 (45%) > Pd@Al_2O_3 (12%) > Pd@C (2%), which shows that Pd NPs supported on SiO_2–NH_2 acted as more active catalysts than those of supported on activated carbon and alumina.

3.3.3. *The catalytic durability of Pd@SiO_2–NH_2 in the catalytic reduction of Cr(VI) to Cr(III)*

The catalytic durability of Pd@SiO_2–NH_2 was evaluated by its isolability and reusability performance tested in the catalytic reduction of Cr(VI) to Cr(III) by using FA at 298 K. For this purpose, after the complete reduction of Cr(VI), Pd@SiO_2–NH_2 catalyst was isolated as black powders, washed with water–ethanol mixture, dried and bottled under nitrogen atmosphere. The isolated Pd@SiO_2–NH_2 catalyst was weighed and re-dispersed in aqueous fresh Cr(VI) solution and yet an active in the catalytic reduction; as given in Fig. 8(a) and (b) Pd@SiO_2–NH_2 catalyst retains >85% of its activity even at the 5th catalytic reuse.

The elemental composition and morphological analyses of reused Pd@SiO_2–NH_2 catalyst were done by BFTEM, ICP-OES analyses and ninhydrin method. Fig. 8(c) shows the BFTEM image of Pd@SiO_2–NH_2 catalyst harvested after 5th catalytic reuse. The size analyses of the resulting Pd NPs (Fig. 8(d)) indicative of a small increase in the average size of Pd NPs throughout the reusability experiments from 3.7 nm (fresh) to 4.2 nm (after 5th reuse), which explains the slight decrease in the observed activity of Pd@SiO_2–NH_2 catalyst. ICP-OES and elemental analyses of the same recovered Pd@SiO_2–NH_2 catalyst gave us almost the identical Pd and $-NH_2$ loading amounts with that of the fresh catalyst. Additionally, the catalytic reduction of Cr(VI) was completely stopped

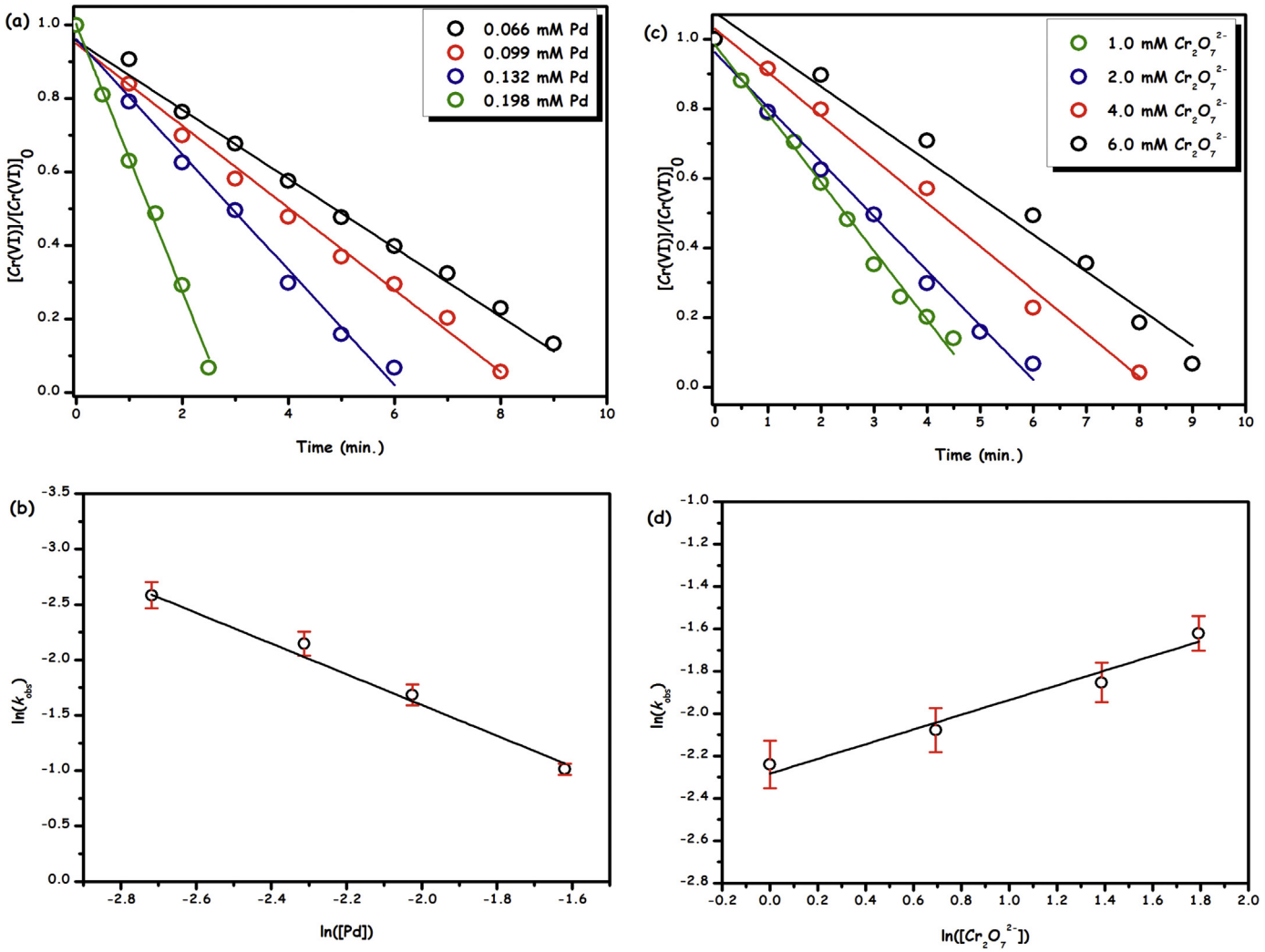

Fig. 10. (a) The remaining fraction of Cr(VI) ($[Cr(VI]/[Cr(VI)]_0$] *versus* time graph for the catalytic reduction of Cr(VI) to Cr(III) ($K_2Cr_2O_7$ 2.0 mM, HCOOH 0.45 M, HCOONa 0.45 M in 10.0 mL H_2O) over Pd@SiO_2–NH_2 catalyst at 298 K and different Pd concentrations, (b) the corresponding observed rate constants *versus* Pd concentration (both in logarithmic scales) graph, (c) the remaining fraction of Cr(VI) ($[Cr(VI]/[Cr(VI)]_0$] *versus* time graph for the catalytic reduction of Cr(VI) to Cr(III) (HCOOH 0.45 M, HCOONa 0.45 M in 10.0 mL H_2O) over Pd@SiO_2–NH_2 (10 mg with 1.40 wt% Pd; 1.32 μmol Pd) catalyst at 298 K starting with different $Cr_2O_7^{2-}$ concentrations, (d) the corresponding observed rate constants *versus* $Cr_2O_7^{2-}$ concentration (both in logarithmic scales) graph.

by the removal of Pd@SiO_2–NH_2 catalyst from the reaction solution; these results confirm the retention of active Pd NPs on the support and no leaching of active catalyst to the solution.

3.4. Kinetic studies for Pd@SiO_2–NH_2 catalyzed reduction of Cr(VI) to Cr(III)

The kinetic studies for Pd@SiO_2–NH_2 catalyzed reduction of Cr(VI) were started by investigating first the effects of FA and SF concentrations on the rate of the catalytic reaction. In this context, the catalytic reduction of Cr(VI) in the presence of Pd@SiO_2–NH_2 catalyst was performed by starting with various initial FA and SF concentrations (Figs. S9 and S10) at 298 K and the results were given as the remaining fraction of Cr(VI) ($[Cr(VI]/[Cr(VI)]_0$] *versus* time graphs (Figs. 9(a) and (c)). Firstly, it was found that the catalytic reaction cannot be proceeding over Pd@SiO_2–NH_2 catalyst without using FA, whereas it undergoes slowly in the absence of SF. The increase in FA concentration up to 450 mM enhances the rate of the catalytic reaction, beyond that concentration the further addition of FA does not boost the rate of catalytic reduction of Cr(VI), which holds almost constant (Fig. 9(b)) like in the case of the saturation kinetics [50]. When we performed the same experiments under identical conditions by just varying SF concentration, we saw that SF plays a promoter role up to 450 mM and the addition of SF more than 450 mM decreases the rate of the catalytic reaction (Fig. 9(d)). The observed drop in the rate of the catalytic reduction can be explained by the poisoning of active Pd centers by formate anion, which electrostatically interacts with metal surfaces [51,52]. In the light of these results FA and SF concentrations were fixed at 450 mM for the further kinetic experiments.

Fig. 10(a) presents the remaining fraction of Cr(VI) ($[Cr(VI]/[Cr(VI)]_0$] *versus* time graphs for the catalytic reduction of Cr(VI) starting with different concentrations of Pd in Pd@SiO_2–NH_2 catalyst at 298 K (Fig. S11). As expected from a preformed catalyst, a linear catalytic reduction starts without induction period and continues until the completion. The observed rate constants (k_{obs}) of catalytic reduction determined from the linear portions of the plots in Fig. 10(a) are in the range of 0.094–0.363 min^{-1}. Plotting the observed rate constants (k_{obs}) *versus* palladium concentration, both in logarithmic scales (Fig. 10(b)), gives a straight line with a slope of 1.18 indicating that the Pd@SiO_2–NH_2 catalyzed reduction of Cr(VI) is first order with respect to the palladium concentration. The effect of substrate concentration [$Cr_2O_7^{2-}$] on the reduction rate was also studied (Fig. S12) by performing a series of exper-

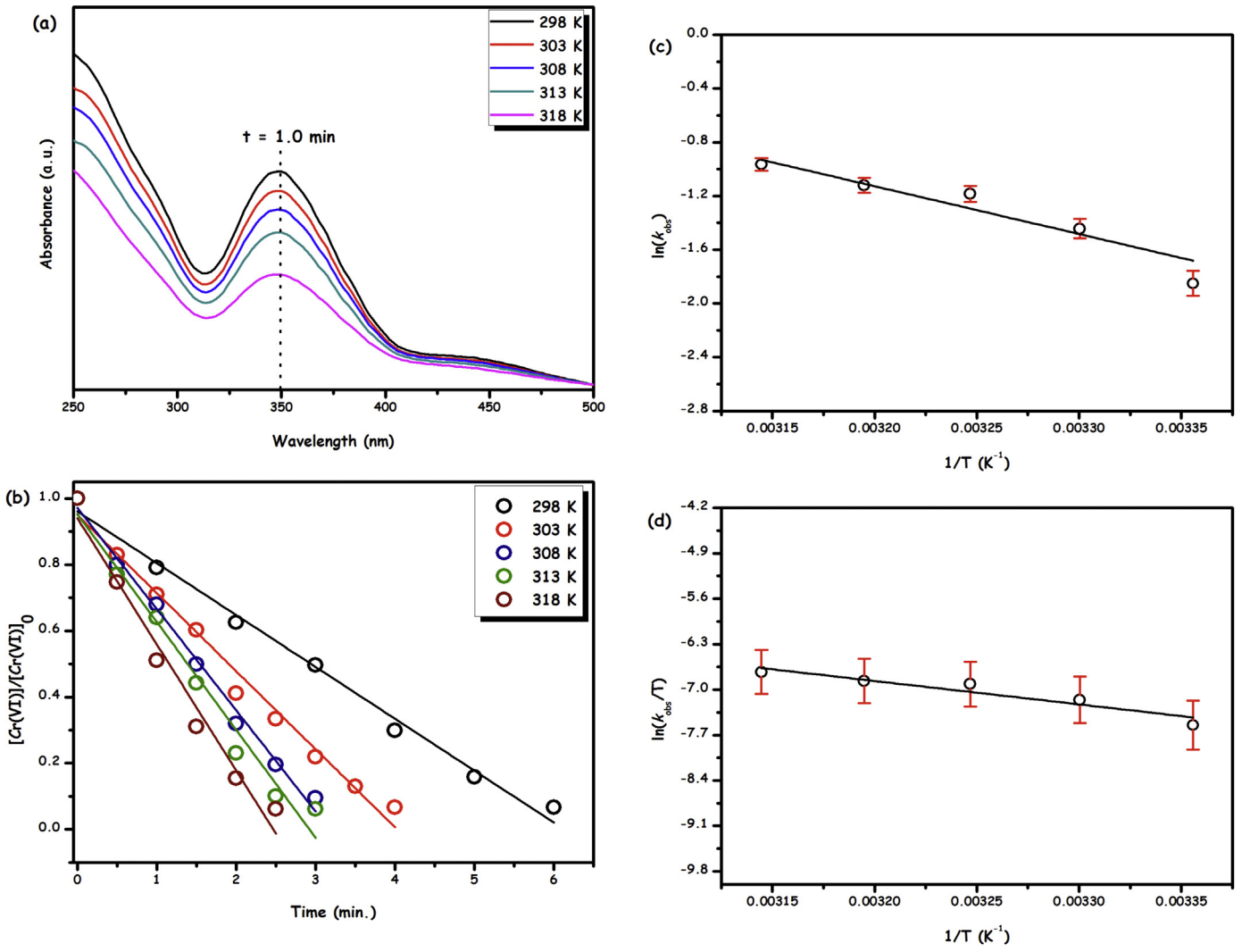

Fig. 11. (a) UV–vis spectra at $t = 1.0$ min. for the catalytic reduction of Cr(VI) to Cr(III) ($K_2Cr_2O_7$ 2.0 mM, HCOOH 0.45 M, HCOONa 0.45 M in 10.0 mL H_2O) over Pd@SiO_2–NH_2 catalyst (10 mg with 1.40 wt% Pd; 1.32 μmol Pd) at different temperatures, (b) the remaining fraction of Cr(VI) ([Cr(VI)]/[Cr(VI)]$_0$] *versus* time graph at different temperatures (298 K–318 K) and corresponding (c) Arrhenius, (d) Eyring-Polonyi plots.

iments starting with varying initial concentration of $K_2Cr_2O_7$ at a fixed catalyst concentration ([Pd] = 0.132 mM). Fig. 10(c) shows the plots of the remaining fraction of Cr(VI) ([Cr(VI)]/[Cr(VI)]$_0$] *versus* time for Pd@SiO_2–NH_2 catalyzed reduction of Cr(VI) at various initial concentrations of Cr(VI) and 298 K. The observed rate constants (k_{obs}) of catalytic reduction of Cr(VI) depending on $Cr_2O_7^{2-}$ concentrations determined from the linear portion of the plots given in Fig. 10(c) were found to be in the range of 0.106–0.198 min^{-1}. The logarithmic plot of these observed rate constants *versus* $Cr_2O_7^{2-}$ concentration gives the line with a slope of 0.47 (Fig. 10(d)) indicative of the catalytic reduction is close to half-order with respect to the dichromate concentration.

In addition to catalyst and substrate concentrations the effect of temperature was also investigated in the Pd@SiO_2–NH_2 catalyzed reduction of Cr(VI) by performing a series of experiments at various temperatures in the range of 298-318 K (Fig. S13). Fig. 11(a) depicts UV–vis spectra of the reaction solutions taken at $t = 1$ min. of these catalytic transformations as expectedly the temperature increase enhances the rate of the catalytic reduction of Cr(VI). Fig. 11(b) presents the remaining fraction of Cr(VI) ([Cr(VI)]/[Cr(VI)]$_0$] *versus* time graphs for the catalytic reduction of Cr(VI) starting at different temperatures. The activity values were found to be 253, 378, 433, 505 and 606 mol $Cr_2O_7^{2-}$/mol Pd min at 298, 303, 308, 313 and 318 K, respectively. These observed activity values are higher than those obtained by Pd tetrapods (4.23 mol $Cr_2O_7^{2-}$/mol Pd min at 323 K) [18], Pd NPs@polymer-nanofibers (2.32 mol $Cr_2O_7^{2-}$/mol Pd min at 323 K) [26] and supported Pd/Pt NPs (1.66 mol $Cr_2O_7^{2-}$/mol Pd min at 318 K) [53]. To the best of our knowledge, the TOF value of 253 mol $Cr_2O_7^{2-}$/mol metal min measured at 298 K is the highest TOF value ever reported for catalytic Cr(VI) reduction at room temperature using a heterogeneous catalyst.

The values of observed rate constants k_{obs} determined from the linear portions of the remaining fraction of Cr(VI) ([Cr(VI)]/[Cr(VI)]$_0$] *versus* time plots at five different temperatures are used to obtain Arrhenius and Eyring plots (Fig. 11(c) and (d)) to calculate activation parameters. Using these plots, apparent activation energy (Ea), apparent activation enthalpy ($\Delta H_a^{\neq}$) and apparent activation entropy ($\Delta S_a^{\neq}$) values were calculated to be 25.9 kJ/mol, 30 kJ/mol and −158.7 J/mol K, respectively. The activation energy obtained by Pd@SiO_2–NH_2 in Cr(VI) reduction is lower than those found by Pd@γ-Al_2O_3 (76.2 kJ/mol) [25] and Pd@TMV (27.3 kJ/mol) [27] catalysts for the same reaction. Assuming that the apparent activation parameters calculated from the macroscopic kinetic data given above are relevant to the most critical activation step Cr(VI) reduction mechanism, one can argue that the positive magnitude of the

apparent activation enthalpy and large negative value of the apparent activation entropy imply the presence of an associative reaction step revealing a transition state.

4. Conclusions

In summary, Pd@SiO_2–NH_2 can simply and reproducibly be prepared by APTS functionalization of SiO_2 support, conventional impregnation of Pd(II) onto this support followed by their borohydride reduction in aqueous solution all at room temperature. The characterization of Pd@SiO_2–NH_2 catalyst was done by using ICP-OES, P-XRD, FTIR, DR/UV–vis, XPS, BFTEM, TEM-EDX and HRTEM, analyses. The results of these multi-pronged analyses reveal the formation of well-dispersed and highly crystalline 3.7 nm Pd NPs on APTS functionalized SiO_2 support. The catalytic performance of Pd@SiO_2–NH_2 in terms of activity and stability was tested in the catalytic reduction of Cr(VI) to Cr(III) by using FA as reducing agent. Pd@SiO_2–NH_2 was found to be highly active nanocatalyst in this catalytic transformation. They provide exceptional turnover frequency (TOF = 258 mol $Cr_2O_7^{2-}$/mol Pd min), which is the highest TOF value among the Pd based heterogeneous employed in the same reaction at room temperature. Moreover, these new Pd NPs show exceptional stability throughout the catalytic runs against leaching and sintering so that they retain >85% of their activity even at the 5th catalytic reuse. Overall, Pd@SiO_2–NH_2 catalyst is available by a simple procedure and is found to be superior heterogeneous catalyst in terms of activity and stability in the hexavalent chromium (Cr(VI)) reduction.

Acknowledgement

MZ thanks to Yüzüncü Yıl University Office of Scientific Research Projects for the financial support to his research laboratory. Additionally, the partial supports by Fevzi Akkaya Scientific Activities Support Fund (FABED), Science Academy and Turkish Academy of Sciences (TUBA) are gratefully acknowledged.

Appendix A. Supplementary data

Supplementary data associated with this article can be found, in the online version, at http://dx.doi.org/10.1016/j.apcatb.2015.06.020

References

[1] S.K. Prabhakaran, K. Vijayaraghavan, R. Balasubramanian, Ind. Eng. Chem. Res. 48 (2009) 2113.
[2] J. Kotas, Z. Stasicka, Environ. Pollut. 107 (2000) 263.
[3] L.H. Keith, W.A. Telliard, Environ. Sci. Technol. 13 (1979) 416.
[4] J.H. Chen, K.C. Hsu, Y.M. Chang, Ind. Eng. Chem. Res. 52 (2013) 11685.
[5] M. Yadav, Q. Xu, Chem. Commun. 49 (2013) 3327.
[6] D.W. Elliott, W. Zhang, Environ. Sci. Technol. 35 (2001) 4922.
[7] D.M. Stearns, L.J. Kennedy, K.D. Courtney, P. Giangrande, L.S. Phieffer, K.E. Wetterhahn, Biochemistry 34 (1995) 910.
[8] World Health Organization, Guidelines for Drinking Water Quality, WHO, Press, Geneva, 2008.
[9] A. Zhitkovich, Chem. Res. Toxicol. 24 (2011) 1617.
[10] H. Kyung, J. Lee, W. Choi, Environ. Sci. Technol. 39 (2005) 2376.
[11] I.J. Buerge, S.J. Hug, Environ. Sci. Technol. 32 (1998) 2092.
[12] Y. Lan, B. Deng, C. Kim, E.C. Thornton, H. Xu, Environ. Sci. Technol. 39 (2005) 2087.
[13] L.C. Hsu, S.L. Wang, Y.C. Lin, M.K. Wang, P.N. Chiang, J.C. Liu, W.H. Kuan, C.C. Chen, Y.M. Tzou, Environ. Sci. Technol. 44 (2010) 6202.
[14] M. Shirzad-Siboni, M. Farrokhi, R.D.C. Soltani, A. Khataee, S. Tajassosi, Ind. Eng. Chem. Res. 53 (2014) 1079.
[15] M. Zahmakiran, S. Özkar, Nanoscale 3 (2011) 3462.
[16] T. Barakat, J.C. Rooke, E. Genty, R. Cousin, S. Siffert, B.L. Su, Energy Environ. Sci. 6 (2013) 371.
[17] M.A. Omole, I.O. K'Owino, O.A. Sadik, Appl. Catal. B 76 (2007) 158.
[18] G.T. Fu, X. Jiang, R. Wu, S.H. Wei, D.M. Sun, Y.W. Tang, T.H. Lu, Y. Chen, ACS Appl. Mater. Inter. 6 (2014) 22790.
[19] L.-L. Wei, R. Gu, J.-M. Lee, App. Catal. B: Environ. (2015), http://dx.doi.org/10.1016/j.apcatb.2015.03.056, Article in Press.
[20] M. Yurderi, A. Bulut, M. Zahmakiran, M. Kaya, App. Catal. B: Environ. 160 (2014) 514.
[21] X. Gu, Z.-H. Lu, H.-L. Jiang, T. Akita, Q. Xu, J. Am. Chem. Soc. 133 (2011) 11822.
[22] M. Yadav, Q. Xu, Energy Environ. Sci. 5 (2012) 9698.
[23] M. Yadav, A.K. Singh, N. Tsumori, Q. Xu, J. Mater. Chem. 22 (2012) 19146.
[24] M. Liang, L. Wang, X. Liu, W. Qi, R. Su, R. Huang, Y. Yu, Z. He, Nanotechnology 24 (2013) 245601.
[25] A. Dandapat, D. Jana, G. De, Appl. Catal. A 396 (2011) 34.
[26] Y. Huang, H. Ma, S. Wang, M. Shen, R. Guo, X. Cao, M. Zhu, X. Shi, ACS Appl. Mater. Inter. 4 (2012) 3054.
[27] C. Yang, J.H. Meldon, B. Lee, H. Yi, Catal. Tod. 233 (2014) 108.
[28] C. Yang, A.K. Manocchi, B. Lee, H. Yi, App. Catal. B: Environ. 93 (2010) 282.
[29] Q.-L. Zhu, Q. Xu, Energ. Environ. Sci. 8 (2015) 478.
[30] M. Yadav, T. Akita, N. Tsumori, Q. Xu, J. Mater. Chem. 22 (2012) 12582.
[31] K. Mori, M. Dojo, H. Yamashita, ACS Catal. 3 (2013) 1114.
[32] A. Bulut, M. Yurderi, Y. Karatas, M. Zahmakiran, H. Kivrak, M. Gulcan, M. Kaya, App. Catal. B: Environ. 164 (2015) 324.
[33] R.J. White, R. Luque, V.L. Budarin, J.H. Clarka, D.J. Macquarrie, Chem. Soc. Rev. 38 (2009) 481.
[34] I. Taylor, A.G. Howard, Anal. Chim. Acta 271 (1993) 77.
[35] E. Abass, M. Alireza, V. Reza, Am. J. Appl Sci. 2 (2005) 1471.
[36] C. Perreira, J.F. Silva, A.M. Perreira, J.P. Araujo, G. Blanco, J.M. Pintado, C. Freire, Catal. Sci. Technol. 1 (2011) 784.
[37] Joint Committee on Powder Diffraction Standards, JCPDS International Center for Diffraction Data, Pennsylvania, 1991.
[38] Y. Zhang, J. Ouyang, H. Yang, Sci. Rep. 3 (2013) 1.
[39] R. Nyholm, N. Maartensson, Solid State Phys. 13 (1980) L279N.
[40] K. Okitsu, H. Bandow, Y. Maeda, Chem. Mater. 8 (1996) 315.
[41] S. Yang, C. Shen, Y. Tian, X. Zhang, H.-J. Gao, Nanoscale 6 (2014) 13154.
[42] U. Schlotterbeck, C. Aymonier, R. Thomann, H. Hofmeister, M. Tromp, W. Richtering, S. Mecking, Adv. Func. Mater. 14 (2004) 999.
[43] N. Su, X. Chen, Y. Ren, B. Yue, H. Wang, W. Cai, H. He, Chem. Commun. 51 (2015) 7195.
[44] S.-M. Kim, Y.-J. Lee, J.-W. Kim, S.-Y. Lee, Thin Solid Films 572 (2014) 260.
[45] S. Enthaler, J.V. Langermann, T. Schmidt, Energy Environ. Sci. 3 (2010) 1207.
[46] M. Zahmakiran, Y.R. Leshkov, Y. Zhang, Langmuir 28 (2012) 60.
[47] A. Roucoux, J. Schulz, H. Patin, Chem. Rev. 102 (2002) 3757.
[48] M. Zahmakiran, M. Tristany, K. Philippot, K. Fajerwerg, S. Özkar, B. Chaudret, Chem. Commun. 46 (2010) 2938.
[49] M. Zahmakiran, M. Tristany, K. Philippot, S. Özkar, B. Chaudret, Dalton Trans. 41 (2012) 590.
[50] K.A. Connors, Theory of Chemical Kinetics, VCH Publishers, New York, 1990.
[51] M. Zahmakiran, S. Ozkar, J. Mol. Catal A: Chem. 258 (2006) 95.
[52] F. Durap, M. Zahmakiran, S. Ozkar, App. Catal. A: Gen. 369 (2009) 53.
[53] M. Liang, R. Su, W. Qi, Y. Zhang, R. Huang, Y. Yu, L. Wang, Z. He, Ind. Eng. Chem. Res. 53 (2014) 13635.